Vignesh Ahilan, Gourav Dhar Bhowmick, Makarand M. Ghangrekar, Michaela Wilhelm, Kurosch Rezwan

# Tailoring hydrophilic and porous nature of polysiloxane derived ceramer and ceramic membranes for enhanced bioelectricity generation in microbial fuel cell

https://doi.org/10.1007/s11581-019-03083-5

# Tailoring hydrophilic and porous nature of polysiloxane derived ceramer and ceramic membranes for enhanced bioelectricity generation in microbial fuel cell

Vignesh Ahilan[1] · Gourav Dhar Bhowmick[2] · Makarand M. Ghangrekar[3] · Michaela Wilhelm[1] · Kurosch Rezwan[1,4]

Received: 18 February 2019 / Revised: 29 March 2019 / Accepted: 21 May 2019

**Abstract**
Selection of proton conducting membrane is currently a key factor that decides the performance of microbial fuel cell (MFC). Uniaxial pressed polysiloxane-derived ceramer and ceramic membrane with proton conducting fillers like montmorillonite and $H_3PMo_{12}O_{40}/SiO_2$ were applied for the first time as separator in MFC. Here, we present a series of polymer-derived ceramic membranes tailored based on pyrolysis temperature and filler addition, in which ion exchange capacity, cation transport number, and oxygen permeability are influenced through the hydrophilic and porous structural property. The maximum power density of MFC with polysiloxane-derived ceramer membrane modified with 20 wt% montmorillonite and 10 wt% $H_3PMo_{12}O_{40}/SiO_2$ reached a value of 5.66 W $m^{-3}$, which was four times higher than that with non-modified polysiloxane-derived ceramer membrane. Furthermore, the specific power recovery per unit cost of the membrane was found to be 2-fold higher than MFC using polymeric Nafion membrane. In contrast, MFC with polysiloxane-derived ceramic membrane modified with 20 wt% montmorillonite delivers 1.2 times lower power density (4.20 W $m^{-3}$) than that with non-modified macroporous polysiloxane-derived ceramic membrane. Hence, the findings demonstrated that tailoring the hydrophilic and porous structure of the ceramic membrane is a new and promising approach to enhance the performance of MFC.

**Keywords** Microbial fuel cell · Porous structure · Hydrophilic nature · Polymer-derived ceramics · Proton exchange membrane

## Introduction

The pollution caused by the use of conventional energy sources represents a serious threat to the existing global ecological system. These stimulate the ongoing research for alternative biochemical energy sources, those that are able to fulfill the future energy demand along with side-aids like wastewater treatment. The microbial fuel cell (MFC) technology is one such alternative energy resources conceptualizing the waste-to-energy principle, which can be used for wastewater treatment with simultaneous recovery of bio-energy using microorganisms as biocatalysts [1, 2]. The recent advances in this field include the increase in the power output due to the advancement in the reactor configuration, utilization of inexpensive electrode and catalyst materials, and modification of the operational regime [3–7]. Nevertheless, achieving high-energy outputs and large-scale applicability of this technique remain a significant challenge, which can be potentially overcome by replacing the mechanically unstable and expensive polymer-based proton-exchange membrane (PEM) like Nafion with low-cost-efficient ceramic membranes [8]. As shown in recent literatures, porous oxide ceramic membranes fabricated from various materials including alumina, mullite, pyrophyllite, and clayware may be potentially utilized for this purpose. For example, the power density of MFCs containing pyrophyllite and clayware ceramic membranes with pore sizes

✉ Michaela Wilhelm
mwilhelm@uni-bremen.de

[1] University of Bremen, Advanced Ceramics, Am Biologischen Garten 2, IW3, 28359 Bremen, Germany

[2] Department of Agricultural and Food Engineering, Indian Institute of Technology Kharagpur, Kharagpur 721302, India

[3] Department of Civil Engineering, Indian Institute of Technology Kharagpur, Kharagpur 721302, India

[4] MAPEX Center for Materials and Processes, University of Bremen, 28359 Bremen, Germany

of 10 μm are 6.93 and 6.85 W $m^{-3}$, respectively [9]. However, Yousefi et al. reported the possibility of bacterial substrate permeation through ceramic membranes with a pore size of around 10 μm, which can limit the overall efficiency of MFC [10]. The average size of bacteria present in the wastewater is above 1 μm. Gubler et al. found that the hydrophilic properties of the ceramic membrane stimulated the proton transmission from the anodic to the cathodic chamber by adsorbed water molecules [11]. Furthermore, the size and distribution of pores in the membrane structure significantly affect the oxygen transport between the cathodic and anodic chambers [12, 13]. The concentration of oxygen in the anodic chamber can lower the efficiency of MFC due to the substrate loss through aerobic respiration by facultative bacteria [14]. The overall performance and durability of MFCs are closely related to the physical properties of their membranes including pore size distribution, hydrophilic properties, ion exchange capacities (IEC), cation transport numbers, and oxygen permeability [15, 16]. Multiple investigations have been performed to develop porous membranes manufactured from canvas, nylon, and cloth, and their power outputs were comparable to those of the commercial Nafion membranes [17, 18].

In the present work, silicon oxycarbide (SiOC) composite materials are investigated as PEM for MFC, owing to their ability to create porous structures and tailorable surface properties [19]. SiOC is a polymer-derived ceramic (PDC), in which polysiloxane polymer precursors undergo thermal decomposition and bond rearrangement, resulting in the formation of amorphous or nanocrystalline ceramics [20]. Unlike the conventional manufacture process of oxide ceramics such as $Al_2O_3$ and $ZrO_2$, which requires heating to very high temperatures (above 1400 °C) [21, 22], PDC membranes can be fabricated by simple pyrolysis under comparatively low-temperature conditions. The complete transformation of the utilized polymer to amorphous SiOC ceramic occurs at temperatures above 800 °C. On the other hand, in the temperature range of 400–800 °C, the product obtained represents a ceramer with partially decomposed functional groups such as methyl and/or phenyl ones. Moreover, several works were published focusing on the ability of polysiloxane polymer to tailor the surface area, surface characteristics, and porous structure of the material [23, 24]. For instance, Prenzel et al. cross-linked polysiloxane polymer with aminopropyltriethoxysilane monomer (APTES) to enhance its hydrophilic properties [25]. In addition, PDC-based composites can be produced by the addition of active or inert filler materials to the polysiloxane matrix, which allows effective tailoring of its physical properties [26].

Recently, Ghadge et al. prepared a clay ceramic membrane composite containing montmorillonite as cation exchange filler and investigated the effects of its pore size, oxygen permeability, and cation transport number on the performance of the manufactured MFC [8]. Fan et al. reported that the proton conductivity of the composite membrane fabricated from the mixture of $H_3PMo_{12}O_{40}$ with Nafion was one order of magnitude higher than that of the commercial Nafion membrane [27]. This is due to the ability of $H_3PMo_{12}O_{40}$ to retain water molecules in its structure, which enhanced the proton conductivity [28]. In our previous investigation, PDC composite membranes containing montmorillonite and $H_3PMo_{12}O_{40}/SiO_2$ fillers were manufactured by the pyrolysis at temperatures of 400, 500, 600, and 1000 °C. It was found that increasing the filler content increased the membrane IEC and cation transport number and decreased its oxygen diffusion coefficient [29].

In this study, PDC membranes were modified with proton-conducting montmorillonite and $H_3PMo_{12}O_{40}/SiO_2$ (phosphomolybdic acid with silica—PMA) fillers at various concentrations and pyrolyzed at 400 and 1000 °C to produce ceramer (PDC:M10-400 and PDC:PMA10:M20-400) and ceramic (PDC:M10-1000) composites, respectively. The surface area, surface characteristics, pore size distributions, IEC, cation transport number, and oxygen diffusion coefficient of the fabricated membranes were measured and compared with those of the materials prepared in our previous work [29] to determine their suitability for applications in MFC. The influential properties of ceramic membrane were investigated for enhanced performance of MFC and evaluated in terms of the generated power density, internal resistance of the MFC, coulombic efficiency (CE), chemical oxygen demand (COD) removal efficiency, and cost comparison analysis. Finally, the performance of MFC with the porous PDC ceramer and ceramic membranes was compared with that of the conventional Nafion membrane under the same operating conditions.

## Materials and methods

### Reagents

Commercial hydrophobic oligomeric methyl-phenyl polysiloxane powder (H44, Silres® Wacker Chemie), monomeric (aminopropyl)triethoxysilane (APTES, ABCR Dr. Braunagel GmbH & Co. KG), montmorillonite K10 (M, Sigma-Aldrich), quaternary dodecyl trimethyl ammonium chloride (97%, Alfa Aesar), phosphomolybdic acid hydrate ($H_3PMo_{12}O_{40}{\cdot}xH_2O$, Alfa Aesar), tetraethylorthosilicate (TEOS, Sigma-Aldrich), hydrochloric acid (37%, Sigma-Aldrich), ethanol (99%, Alpha Aesar), ammonia solution (25%, VWR Chemicals), and deionized water (D.I.) were used for membrane preparation.

### Membrane synthesis procedure

PMA filler ($H_3PMo_{12}O_{40}/SiO_2$) and PDC-based composite membranes were synthesized by a sol-gel and pressing method, respectively, as explained in detail elsewhere [29]. In brief, 1.99 g of quaternary dodecyl trimethyl ammonium chloride

was dissolved in 200 mL of HCl solution (25%) followed by the addition of 17.83 mL of TEOS and 4.69 g of $H_3PMo_{12}O_{40}\cdot xH_2O$ under stirring for 1 h. The resulting mixture was aged at room temperature for 4 h and then separated by centrifugation, thoroughly washed with ethanol, and dried inside an oven at 80 °C for 24 h. The fillers were dispersed in ethanol for 30 min by ultrasonication. A mixture of H44 and APTES was dissolved in the produced dispersion and subjected to polymerization under reflux for 3 day at 70 °C using a mixture containing 3.27 mL of ammonia solution and 3 mL of D.I. water. After removing the solvent and drying at 140 °C, the product obtained was thermally cross-linked in air at 200 °C for 2 h, ground into fine powder, and pressed into monolithic green bodies. The produced samples were pyrolyzed under nitrogen atmosphere at 400 °C and 1000 °C to obtain round-shaped ceramer and ceramic membranes, respectively.

## Sample notation

Sample nomenclature was based on the notation PDC:PMAxx:Myy–zzz, where PDC represents SiOC, PMA stands for $H_3PMo_{12}O_{40}/SiO_2$ (phosphomolybdic acid with silica) with weight fraction xx, *M* denotes montmorillonite with weight fraction yy, and zzz is the pyrolysis temperature (in °C). The sample compositions and their nomenclatures are listed in Table 1.

## Material characterization

Brunauer–Emmett–Teller (BET)-specific surface area was measured by recording nitrogen adsorption and desorption isotherms at 77 K (Belsorp-Mini, Bel Japan). The samples were heated at 120 °C for 3 h as a pretreatment in order to remove adsorbed water molecules from the material surface. Particle sizes, porosity, and mean pore sizes of the samples were measured via mercury intrusion porosimetry (Pascal 140/440, Porotec). Vapor adsorption studies were performed by placing 0.5 g of dry PDC composite powders into closed Erlenmeyer flasks filled with water or heptane solvent in equilibrium with its vapor phase at room temperature. The samples were weighed before and after a 24-h measurement period to determine the amount of adsorbed vapors. Finally, the adsorption capacities of the membranes were calculated by taking into account their specific surface areas determined via the BET method.

## Ion exchange capacity

The IEC of each membrane was determined by titration method [30]. First, the membrane was equilibrated by soaking in 100 mL of 1 M HCl solution for 72 h, after which it was rinsed with D.I. water to remove the adsorbed ions from the membrane surface and transferred to 50 mL of 1 M NaCl solution for 24 h to exchange $H^+$ and $Na^+$ ions during equilibration. Finally, the membrane was removed from the reaction system, and the remaining medium was titrated with 0.005 M NaOH solution to determine the amount of $H^+$ ions present. The IEC obtained was expressed in milliequivalents of $H^+$ per gram of dry membrane as per Eq. (1).

$$\mathrm{IEC} = (V_{\mathrm{NaOH}} \times M_{\mathrm{NaOH}})/W_{\mathrm{dry}} \quad (1)$$

where $V_{\mathrm{NaOH}}$ is the volume of the NaOH solution consumed, $M_{\mathrm{NaOH}}$ is the molarity of NaOH (0.005 M), and $W_{\mathrm{dry}}$ is the weight of the dry sample.

## Cation transport number

The cation transport number ($t^+$) was estimated using a dual-chamber tank, whose anode and cathode chambers were filled with 0.5 and 0.005 M NaCl solutions, respectively, to create an osmotic drag concentration gradient. Two identical Ag/AgCl reference electrodes were used to monitor the potential difference between the closest points of the membrane sides over time. The value of $t^+$ was estimated using Eq. (2).

$$E_{\mathrm{v}} = \frac{\mathrm{RT}}{\mathrm{F}}(2t-1)\ln\left(\frac{\mathrm{C1}}{\mathrm{C2}}\right) \quad (2)$$

where $E_{\mathrm{v}}$ is the potential difference at the nearest point of the membrane (mV), *R* is the gas constant, *F* is the Faraday's constant (C $mol^{-1}$), *T* is the temperature (K), $t^+$ is the cation transport number, C1 is the anode chamber concentration

**Table 1** Prepared membrane compositions and their particle size of cross-linked sample after ball milling

| Membranes | Montmorillonite *M* (wt%) | $H_3PMo_{12}O_{40}/SiO_2$ PMA (wt%) | Particle size (μm) |
|---|---|---|---|
| PDC | – | – | 5.8357 |
| PDC:M10 | 10 | – | 3.8642 |
| PDC:M20 | 20 | – | 3.6574 |
| PDC:PMA10:M10 | 10 | 10 | 2.5328 |
| PDC:PMA10:M20 | 20 | 10 | 2.2254 |

(0.5 M), and C2 is the cathode chamber concentration (0.005 M).

## Oxygen permeability

The oxygen diffusion coefficients of the produced membranes were measured by filling the chamber 1 with D.I. water and purged with $N_2$ gas for 30 min to reach the anaerobic state with an oxygen concentration of $< 0.02$ mg $L^{-1}$, whereas chamber 2 (also filled with D.I. water) was aerated continuously to maintain a near-saturation level of dissolved oxygen (DO). The oxygen concentration in the chamber 1 chamber was monitored at regular intervals of 15 min using a DO probe, and the oxygen mass transfer and diffusion coefficients were estimated using Eqs. (3) and (4), respectively.

$$k_o = -\frac{v}{At}\ln\frac{C_{oc}-C_{oa}}{C_{oc}} \quad (3)$$

$$D_o = K_o \times L_{th} \quad (4)$$

where $v$ is the volume of the chamber ($cm^3$), $A$ is the area of the membrane ($cm^2$), $t$ is the time (s), $C_{oc}$ is the oxygen concentration at chamber 2, $C_{oa}$ is the oxygen concentration at chamber 1, $K_o$ is the oxygen mass transfer coefficient, $D_o$ is the oxygen diffusion coefficient, and $L_{th}$ is the thickness of the membrane.

## Microbial fuel cell setup and operation

Six numbers of MFCs were fabricated by 30-mm thick poly-(methyl-methacrylate) fiber sheet with a working volume for the anodic and cathodic chambers of 100 mL each (Scheme 1). The Nafion membrane, with projected surface area of 4.9 $cm^2$, was used as a PEM for the control MFC after pre-treating with 3% $H_2O_2$ solution for 1 h to remove the presence of organic impurities followed by dipping in D.I. water for 2 h to remove the residual $H_2O_2$ and boiling in 0.5 M $H_2SO_4$ for 1 h followed by dipping in D.I. water for another 1 h to activate the sulfonate groups ($SO_3^-$) in the membrane [31]. The pieces of carbon felts used as the anode and cathode with the projected surface area of 25 $cm^2$ each were pre-treated by a sequence of washing with 1 N $HNO_3$, 30% ethanol, and D.I. water until reaching the neutral pH, followed by drying in a hot air oven at 100 °C. The dried carbon felt pieces were subjected to thermal treatment in a muffle furnace at 400 °C for 30 min and then stored in vacuum desiccators for further use after cooling. The carbon felts are pre-treated in order to make sure that it is free from initial microbial contamination, which can alter the performance of MFC. On the other hand, the pre-treatment alters surface characteristics towards a more hydrophilic surface for effective biofilm growth, since the hydrophobic nature of untreated carbon felt restricts the development of biofilm [32]. The anode and cathode were connected with concealed copper wires, and the membranes were glued to a Teflon gasket sheet using specified proportions of water-resistant resin and glue.

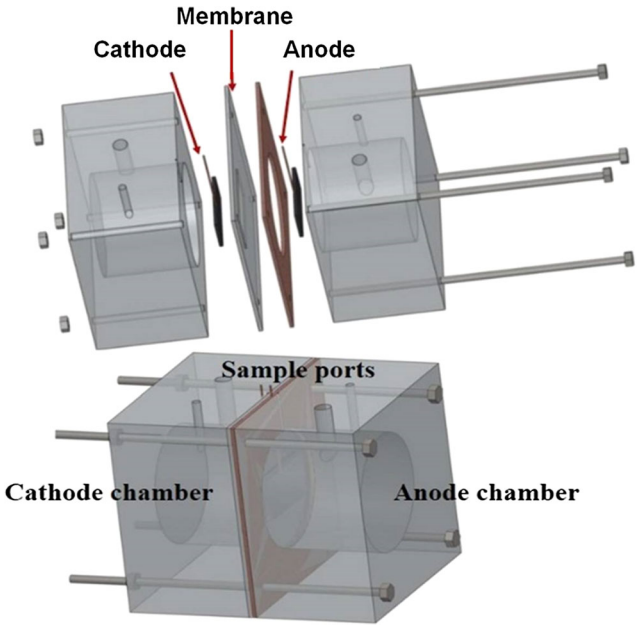


**Scheme 1** Schematic diagram of the MFC set-up

The operating voltage (OV) was measured over a 100-Ω external resistance. Six MFCs with PDC-400, PDC:PMA10:M10-400, PDC:PMA10:M20-400, PDC-1000, PDC:M20-1000, and Nafion were labeled as MFC-1, MFC-2, MFC-3, MFC-4, MFC-5, and MFC-6, respectively. The MFCs were inoculated with anaerobic mixed consortia collected from a septic tank at the Indian Institute of Technology, Kharagpur after heat pre-treatment (100 °C for 15 min) with volatile and total suspended solids concentrations of 19.9 and 30.2 g $L^{-1}$, respectively. Synthetic wastewater with sucrose as a carbon source was supplied as the feed for all MFCs. The feed composition was adopted from the work of Jadhav et al. with an organic matter concentration of around 3 g of COD $L^{-1}$ supplemented with trace nutrients and having pH of 7.4 [33]. All MFCs were operated in an open environment with ambient temperature of 28 ± 2 °C. MFCs were operated under batch mode at a fresh feeding frequency of 3 days and to verify the precision of the results each MFC was operated for 15 feed cycles to achieve representative performance results.

## Analytical measurements

The potential values and generated currents were measured using a digital multi-meter with a data acquisition unit (Agilent Technologies, Malaysia). Polarization was performed

by varying the external resistances from 10,000 to 10 Ω using a variable resistance box (GEC 05 R Decade, Renown Systems, Kolkata, India), and the corresponding stable voltages at all external resistances were recorded at 30-min time intervals using a data acquisition unit connected to a personal computer. Normalized volumetric power density was expressed with respect to the volume of anodic chamber according to Eq. (5).

$$\mathrm{PV,max} = \frac{V^2}{Rv_{an}} \tag{5}$$

where $P_{\mathrm{V,max}}$ is the volumetric power density (W $m^{-3}$), $V$ is the acquired voltage (V), $R$ is the external resistance (Ω), and $v_{an}$ is the volume of anodic chamber ($m^3$).

The total internal resistance of the MFC was estimated from the slope of the linear portion of the polarization plot (voltage vs. current density). Coulombic efficiency (CE) was calculated by integrating the measured current over time with respect to the maximum available coulombs associated with the organic matter via Eq. (6) [34].

$$\mathrm{CE} = \frac{M_s \int_0^t I\,dt}{\mathrm{F}b_{es}V_{An}\Delta\mathrm{COD}} \tag{6}$$

where $M_s$ is the molecular weight of the substrate (g $mol^{-1}$), ΔCOD is the change in the substrate concentration over a batch cycle (g $L^{-1}$), $V_{An}$ is the liquid volume of the anodic chamber (L), $F$ is Faraday's constant (96,485 C $mol^{-1}$), and $b_{es}$ is the molar amount of electrons generated during the oxidation of 1 mol of substrate (mol of $e^-$ mol of substrate$^{-1}$). For the samples collected from the anodic chamber of MFCs at regular time intervals, COD values were estimated by a closed reflux method according to the procedure described in Standard Methods [35]. Normalized energy recovery (NER) was also assessed and expressed based on the volume of wastewater treated over time (kWh $m^{-3}$) as per Eq. (7) [36].

$$\mathrm{NER}\left[\mathrm{kWh/m^3}\right] = \frac{\mathrm{Energyoutput}}{\mathrm{Treatedwastewatervolume}} \tag{7}$$

The power recovery from MFCs using different membranes was analyzed in terms of the corresponding power/cost ratio as per Eq. (8) [37].

$$\mathrm{Powerrecovery} = \frac{P_s\left(\frac{\mathrm{mw}}{\mathrm{m^2}}\right)}{\mathrm{Cost}\left(\frac{/\mathrm{EUR}}{\mathrm{m^2}}\right)} \tag{8}$$

where $P_s$ is the power density (based on membrane surface area) of the MFC and Cost is the cost per unit area of the membrane.

## Results and discussion

### Micro-/meso- and macro-pore structure

The physical characteristics of PDC:M10-400 and PDC:PMA10:M20-400 ceramers and the PDC:M10-1000 ceramic membranes synthesized in this study were examined and compared with those of the materials discussed in our previous study. The macropore sizes of the membranes and their distributions determined by the mercury intrusion method are shown in Fig. 1a, b. The fabrication of membranes with pore sizes smaller than 1000 nm is beneficial for preventing the migration of bacterial substrate from the anodic to the cathodic chamber. The resulting membrane pore sizes ranged between 100 and 1000 nm depending on the material composition; for instance, the ceramer-based samples exhibited average pore sizes ranging from 200 to 650 nm, whose magnitudes decreased with increasing contents of montmorillonite and PMA fillers. Similarly, the average pore size of the PDC ceramic membrane decreased from 760 to 420 nm after the addition of 20 wt% montmorillonite (PDC:M20-1000), owing to the decrease in the particle sizes of the pre-pyrolyzed powders (Table 1). Meanwhile, the average pore size of PDC:PMA10:M20-400 ceramer was equal to 316 nm, and its open porosity was 39%. Higher value of the open porosity of a hydrophilic membrane helps to retain a large amount of water molecules, which enhance the proton transfer characteristics of the MFC.

The BET-specific surface areas of the resulting ceramers were strongly affected by the micro- and mesoporous structures of montmorillonite and PMA fillers. The nitrogen adsorption–desorption isotherm curves are shown in Fig. 1c. In particular, PDC:PMA10:M20-400 ceramer was characterized by the highest specific surface area of 124 $m^2$ $g^{-1}$ as compared to the values obtained for the other tested materials and bare PDC ceramer membrane (Fig. 1d). These results suggest that the ceramer containing both montmorillonite and PMA fillers exhibits a hierarchical (micro/meso/macro) pore structure. Xu et al. found that the formation of mesopores in metal organic framework and covalent organic framework materials enhanced their proton conductivity properties as compared to those of non-porous membranes [38]. Moreover, the presence of a hierarchical (micro/meso/macro) pore structure in the membrane material inhibits the migration of dissolved oxygen (DO) from the cathodic to the anodic chamber, which improves its overall efficiency. However, all ceramic membranes (pyrolyzed at 1000 °C) investigated in this study do not have any micro- or mesopores (including the PDC:M20-1000 ceramic membrane with a specific surface area of 4.2 $m^2$ $g^{-1}$), which could be explained by the collapsing of the layered aluminate–silicate montmorillonite structure and complete transformation of organic molecules to SiOC species at high pyrolysis temperatures. Hence, the ceramic

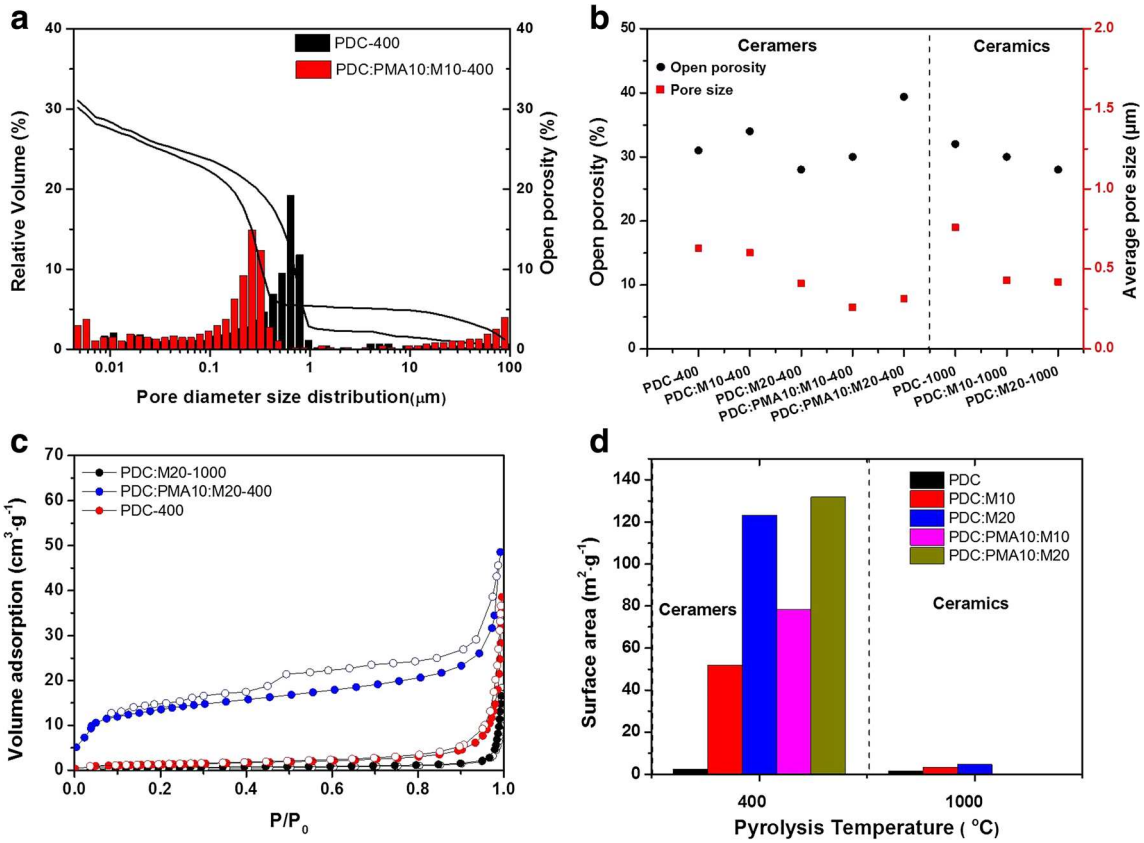


**Fig. 1** (**a**) Pore size distribution versus relative pore volume and open porosity curves obtained from Hg-porosimetry histogram of pyrolyzed samples. (**b**) Average pore size and open porosity versus as prepared PDC membranes plot. (**c**) Nitrogen adsorption–desorption isotherms of montmorillonite and $H_3PMo_{12}O_{40}/SiO_2$ functionalized PDC membranes, pyrolyzed at 400 and 1000 °C. (**d**) Specific surface areas of pyrolyzed (400 and 1000 °C) membranes as determined by nitrogen adsorption–desorption isotherm

SiOC membranes possess only macroporous structures, which can also promote proton diffusion from one chamber to the other.

## Hydrophilic/hydrophobic characteristics

The water and heptane adsorption characteristics of the prepared membranes were examined to elucidate their hydrophilic/hydrophobic properties (Fig. 2a, b). The obtained adsorption capacities were found to be dependent on the specific surface areas of the studied materials and determined by recording nitrogen adsorption–desorption isotherms. The degree of hydrophilicity of a material is correlated with the water/heptane adsorption ratio; when its magnitude is greater than one, it is considered hydrophilic despite its intrinsic hydrophobicity. The observed hydrophobic behavior of the produced ceramer membranes can be attributed to the partial decomposition of methyl and phenyl functional groups in the H44 polysiloxane matrix. In this study, the addition of montmorillonite to the PDC matrix did not apparently affect the water/heptane adsorption ratios of the ceramer membranes. However, the addition of PMA filler led to the formation of the highly hydrophilic PDC:PMA10:M10-400 and PDC:PMA10:M20-400 ceramer structures, owing to the hygroscopic nature of PMA that was capable of retaining water molecules inside its micro- and mesopores. The PDC-1000, PDC:M10-1000, and PDC:M20-1000 ceramic materials exhibited hydrophilic properties because of the complete decomposition of their methyl and phenyl functional groups into SiOC species during pyrolysis at 1000 °C. Such hydrophilic behavior helps to retain water molecule in the membrane structure, which promotes the transfer of protons from the anode to the cathode chamber.

## Ion exchange capacity

The IEC values of the ceramer membranes demonstrated stepwise increases with the addition of montmorillonite to the PDC matrix (Fig. 3a) due to the presence of a charged interlayer between the aluminate and silicate layers in the montmorillonite structure. Moreover, the addition of both PMA and montmorillonite fillers to PDC dramatically increased the IECs of the ceramer membranes by a factor of six. The ion transfer process in the membrane structure was caused by the proton hopping between various hydroxyl groups or water molecules adsorbed on the porous membrane surface.

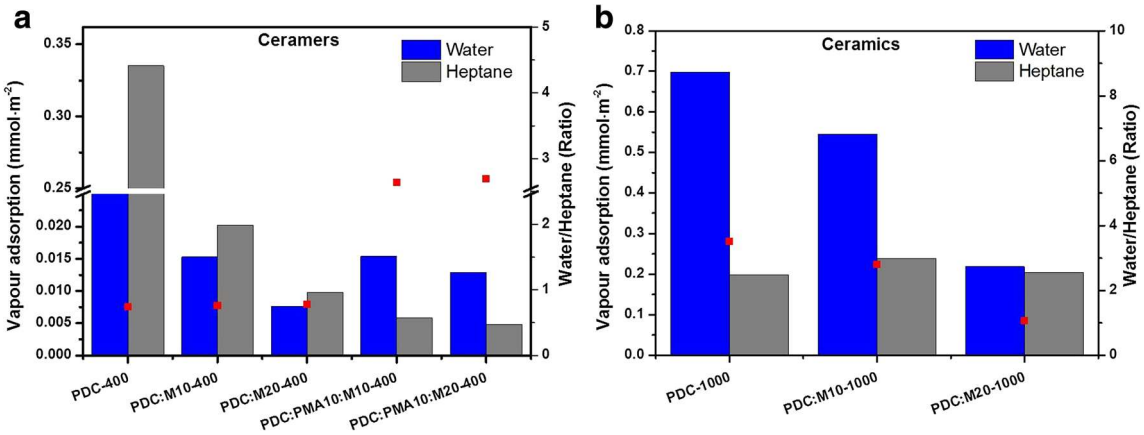


**Fig. 2** Water and n-heptane vapor adsorption at 25 °C and ratio of hydrophilic and hydrophobic nature. (**a**) Ceramer membranes. (**b**) Ceramic membranes

Meanwhile, the addition of montmorillonite and PMA fillers facilitated the proton transfer by charged ions in the membrane structure. However, the ceramic membranes exhibited completely different behavior: Their IEC values decreased with increasing montmorillonite content, which resulted not only from their lower degrees of hydrophilicity but also from the collapse of the charged interlayer structure of montmorillonite filler after the pyrolysis at 1000 °C [29].

## Cation transport number

The cationic transport number (Fig. 3b) of PDC and montmorillonite-modified PDC ceramers is comparable to each other because both materials exhibit hydrophobic properties. The addition of PMA and montmorillonite fillers to the PDC matrix dramatically increased the cation transport number of the membrane due to the mesoporous structure of PMA. Higher cation transport numbers were obtained for the PDC:PMA10:M20-400 (0.7028) and PDC:PMA10:M10-400 (0.6928) ceramer membranes because of their good hydrophilic properties and smaller pore sizes. Daiko et al. elucidated the ion transport mechanism in hydrophilic porous structures by adsorbing water molecules, which formed passages for ion hopping at low activation energies and high ionic conductivity [39]. The cation transport number of the fabricated ceramic membranes was observed to be in the decreasing order as PDC-1000, PDC:M10-1000, and PDC:M20-1000, owing to the gradual changes of their hydrophilic properties.

## Oxygen permeability

Presence of separator in MFC prevents the diffusion of DO from the aerobic cathodic chamber to the anaerobic anodic chamber. The oxygen diffusion coefficients of the membranes fabricated in this study are shown in Fig. 3c. According to Li et al., pore structure and open porosity of the membrane significantly influence the diffusion of DO in the MFC systems [40]. The PDC ceramer membrane investigated in this work was characterized by the average pore size of 630 nm and oxygen diffusion coefficient of $2.41 \times 10^{-4}$ $cm^2$ $s^{-1}$, which decreased to $1.77 \times 10^{-4}$ $cm^2$ $s^{-1}$ after the addition of 20 wt% montmorillonite due to the reduction of the average pore size of the SiOC matrix to 410 nm. Furthermore, after the addition of both PMA and montmorillonite fillers, the PDC:PMA10:M20-400 ceramer membrane exhibited the minimal oxygen diffusion coefficient of $1.72 \times 10^{-4}$ $cm^2$ $s^{-1}$ and average pore size of 316 nm while retaining the open porosity of 39%, which could be mainly attributed to the mesoporous Keggin structure of PMA. The observed low degree of oxygen permeation through the PDC:PMA10:M20-400 ceramer membrane might be due to the presence of a randomly oriented micro/mesoporous structure in the macropore architecture. Meanwhile, the minimal DO diffusion coefficient was obtained for the PDC ceramic membrane (as compared to that of PDC:M20-1000 ceramic), because the surface characteristic of the PDC:M20-1000 membrane was less hydrophilic and possessed higher oxygen permeability, owing to the nonpolar nature of oxygen molecules. Similarly, Atwater et al. reported that the hydrophilic properties of the membrane inhibited the permeation of DO through the membrane due to their non-polar characteristics [41].

## Power generation

Three ceramer and two ceramic membranes were selected based on their physical properties such as surface area, water/heptane ratio, IEC, cation transport number, and oxygen permeability. In particular, the hierarchical (micro/meso/macro) pore structured PDC:M10:PMA10-400 and PDC:M10:PMA20-400 ceramer membranes exhibited high degrees of hydrophilicity, IECs, and cation transport numbers as well as low oxygen permeabilities as compared with those of the other ceramer membranes pyrolyzed at 400 °C. Meanwhile, the macropore-structured PDC-400 ceramer,

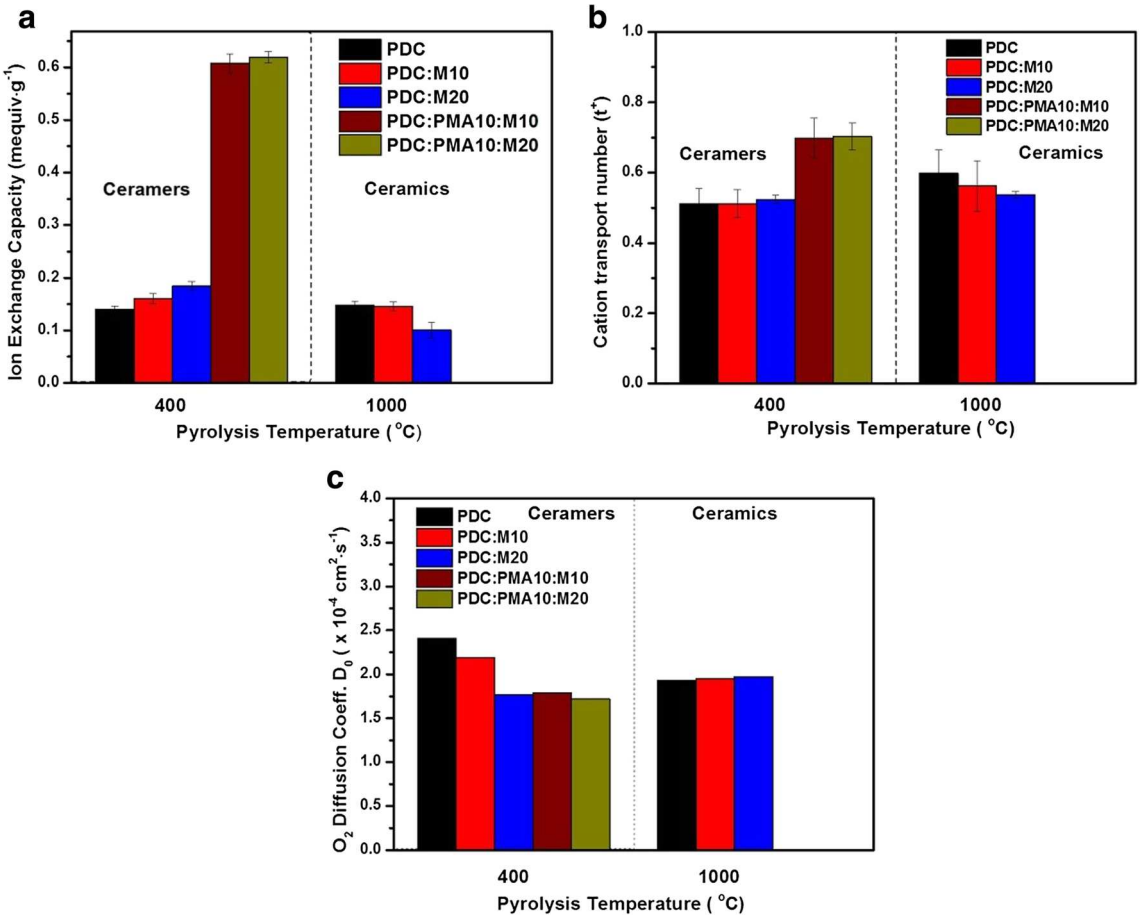


**Fig. 3** (**a**) Ion exchange capacity measured for as prepared ceramer and ceramic membranes. (**b**) Cation transport number of ceramic membrane. (**c**) Oxygen diffusion coefficient of PDC membranes

PDC-1000, and PDC:M20-1000 ceramic membranes were also studied as membrane materials for MFCs to understand the significance of membrane hydrophilic and porous structural properties.

The electrical performance of the fabricated MFCs was evaluated in terms of generated voltages and power density. Their magnitudes were determined by measuring the OV and open-circuit voltage (OCV) from the day of activation of MFC confirming the presence of active electrogenic bacteria in the septic tank mix consortia. The average OV of 224.5 ± 6.5 mV was achieved for the MFC-3 with PDC:PMA10:M20-400 membrane under steady-state operating conditions corresponding to an external resistance of 100 Ω, which exceeded the values obtained for the MFC-1 with the PDC-400 membrane (86.3 ± 3.4 mV) and MFC-6 with a polymeric Nafion membrane (186.0 ± 6.5 mV). The internal resistances of the MFCs resulting from the overpotential losses of their electrodes as well as because of the ohmic resistances of the membrane–electrolyte interfaces were measured from the slopes of the linear portions of the voltage versus current curves. The MFC-3 was characterized by the lowest internal resistance of 138 Ω followed by the MFC-2 (142 Ω) and MFC-4 (151 Ω) (Fig. 4a), which are mainly dependent on the ion transport capability of the membrane. In addition, polarization was conducted for MFCs containing different membranes to compare their overall volumetric power densities. Among various MFCs with the as-synthesized and commercial membranes, MFC-3 demonstrated the best performance corresponding to the maximum volumetric power density ($P_{V,max}$) of 5.66 W $m^{-3}$, which was 4-fold higher than MFC-1 with PDC-400 ceramer membrane. On the other hand, the OV and $P_{V,max}$ of 157.7 ± 5.61 mV and 5.10 W $m^{-3}$ were achieved for the MFC-4 with PDC-1000 membrane material; these values were 24.4 and 21.6% higher than that obtained for MFC-5 with the PDC:M20-1000 membrane, respectively. Moreover, the current density of the MFC-4 (1013 mA $m^{-2}$) was 1.6 times greater than that of the MFC-5 with PDC:M20-1000 membrane. The maximum volumetric power and current densities obtained for the fabricated MFCs can be ranked as follows: MFC-3 > MFC-6 > MFC-2 > MFC-4 > MFC-5 > MFC-1 (Fig. 4b).

From these results, it can be concluded that the MFC-3 with the PDC:PMA10:M20-400 ceramer membrane exhibits the highest power generation proficiency as compared to those of

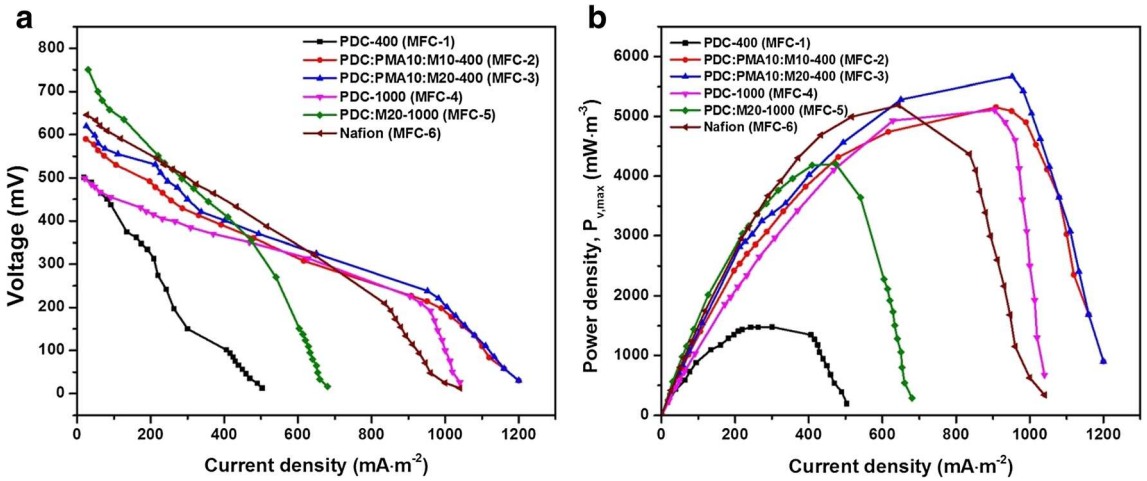


**Fig. 4** (**a**) Polarization curve. (**b**) Power density curves

the other membranes due to its highly hydrophilic properties that facilitates capturing water molecules in the membrane structure. These water molecules act as carriers for protons diffusing from the anodic to the cathodic chamber in the form of hydronium ($H_3O^+$) clusters under the action of osmotic and electroosmotic drag forces. In addition to that, the presence of hierarchical (micro/meso/macro) pores in the PDC:PMA10:M20-400 and PDC:PMA10:M10-400 ceramer membranes inhibits the migration of oxygen molecules from the cathodic to the anodic chamber. On the other hand, MFC-1 with PDC-400 ceramer membrane showed the lowest power generation among all other MFCs. This is due to the hydrophobic characteristics and bigger pore size that lead to diffusion of higher concentration of oxygen to the anodic chamber, which significantly reduces the performance of MFC. Meanwhile, the MFC-4 with PDC-1000 membrane generated higher power and current densities as compared to that of the MFC-5 with PDC:M20-1000 membrane. This is mainly because of higher hydrophilicity behavior of PDC-1000 ceramic membrane. Although the hydrophilicity of the PDC-1000 ceramic membrane is higher than that of the PDC:PMA10:M20-400 ceramer membrane, the power generation of the MFC-4 with PDC-1000 is lower than that of the MFC-3 with PDC:PMA10:M20-400 because of the presence of a hierarchical pore structure in PDC:PMA10:M20-400, which inhibits the permeation of oxygen molecules through the membrane. The physical characteristics of the prepared membrane materials, including their surface areas, pore structures, hydrophilic properties, IECs, cation transport numbers, and oxygen diffusion coefficients, were in good agreement with the performance results of MFCs.

## Wastewater treatment

Wastewater contains complex macromolecules, which are easily degraded in the presence of various bacteria in the anaerobic inoculum. The electrogenesis step of the wastewater treatment procedure is preceded by fermentation, during which complex macromolecules such as polysaccharides undergo fermentation and are ultimately reduced to simpler carbon chain compounds. A fraction of the reduced substrate is

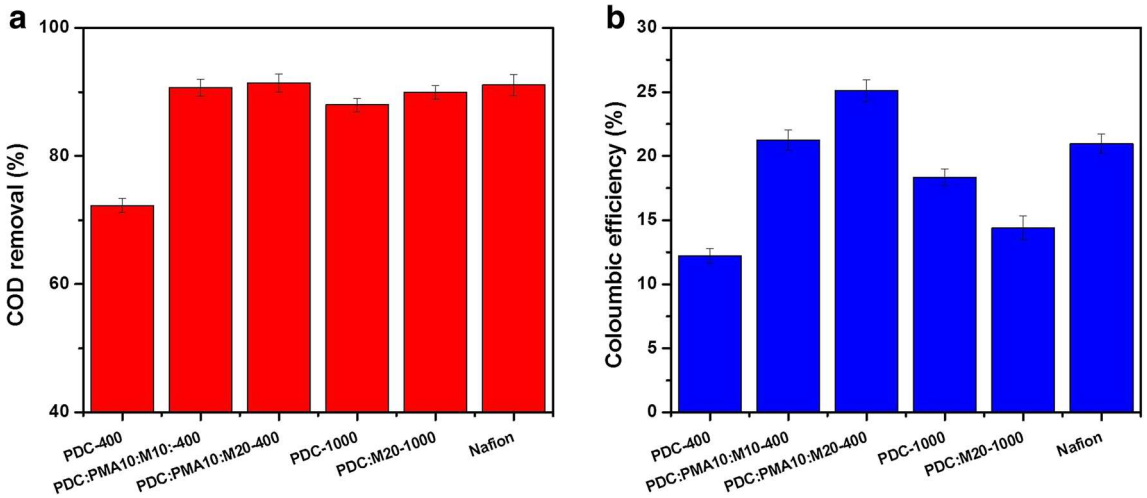


**Fig. 5** (**a**) COD removal efficiency. (**b**) Coulombic efficiency of MFCs

**Table 2** Performance comparison of PDC membranes with polymeric and ceramic membranes

| Membranes | Anode | Cathode | Power density, $P_{V,max}$ (mW m$^{-3}$) | Membrane cost (€ m$^{-2}$) | Power recovery (mW €$^{-1}$) | Coulombic efficiency (%) | NER (kWh m$^{-3}$) | COD removal (%) |
|---|---|---|---|---|---|---|---|---|
| PDC-400 (MFC-1) | Carbon felt | Carbon felt | 1479.2 | 1066.8 | 0.282 | 12.2 | 0.106 | 72. 3 |
| PDC:PMA10:M10-400 (MFC-2) | Carbon felt | Carbon felt | 5152.9 | 1112.9 | 0.944 | 21.2 | 0.371 | 90.7 |
| PDC:PMA10:M20-400 (MFC-3) | Carbon felt | Carbon felt | 5664.4 | 1015.54 | 1.09 | 25.1 | 0.407 | 91.4 |
| PDC-1000 (MFC-4) | Carbon felt | Carbon felt | 5107.6 | 1066.8 | 0.97 | 18.3 | 0.367 | 88.0 |
| PDC:M20-1000 (MFC-5) | Carbon felt | Carbon felt | 4200.8 | 984.6 | 0.87 | 14.4 | 0.302 | 90.0 |
| Nafion (MFC-6) | Carbon felt | Carbon felt | 5184.2 | 1943 | 0.54 | 20.9 | 0.373 | 91.1 |
| PVA-STA/GO [42] | Carbon cloth | Carbon cloth/Pt-C | 1190 | – | – | 3.3 | – | 83.7 |
| Polybenzimidazole/SBA15 [43] | Carbon paper | Carbon cloth | 1521.0 | – | – | – | – | 78.0 |
| Mullite [9] | Carbon veil | Carbon veil | 4980.0 | – | – | – | – | 41.5 |
| Alumina [9] | Carbon veil | Carbon veil | 2600.0 | – | – | – | – | 49.4 |
| Earthernware [44] | Graphite plate | Stainless steel mesh | 3800.0 | – | – | 19.8 | – | – |
| Coconut shell [18] | Carbon felt | Carbon felt | 3200 | – | – | 16.5 | – | 66.0 |
| Nylon (10-μm pore size) [17] | Carbon cloth | Carbon cloth | 769 ± 65 mW m$^{-2}$ | – | – | 55 | – | – |
| Glass fiber filter (1-μm pore size) [17] | Carbon cloth | Carbon cloth | 716 ± 60 mW m$^{-2}$ | – | – | 60 | – | – |

consumed by microbes, while the rest is converted into electrons and protons, leading to power generation. During the stable phase of operation, all MFCs demonstrated COD removal efficiencies ranging from 72 to 92%. In particular, specific COD removal efficiency values of 72.3 ± 1.1, 90.7 ± 1.3, 91.4 ± 1.4, 88.0 ± 1.1, 90.0 ± 1.0, and 91.1 ± 1.7% were achieved by the MFC-1, MFC-2, MFC-3, MFC-4, MFC-5, and MFC-6, respectively (Fig. 5a). Highest COD removal was observed for the MFC-3, which could be attributed to the large IEC value, good pore size distribution, and other physical characteristics of the PDC:PMA10:M20-1000 ceramer membrane, which preserved the microenvironment in the vicinity of the anode by promoting the scavenging of electrons and protons from the anodic chamber of MFC to the cathodic chamber.

The CE of the MFC-3 (25.1 ± 0.8%) was also substantially higher than other MFCs, including the MFC-6 containing a commercial polymeric Nafion membrane (Fig. 5b), indicating that a larger fraction of organic matter was effectively consumed by the electrogenic bacteria during oxidation in the MFC-3. This phenomenon can be explained by the porous structure of the ceramer membrane and its superior physical properties, such as the relatively high IEC and cation transfer number and low oxygen permeability coefficient. Overall, the MFC-3 containing a PDC:PMA10:M20-400 ceramer separator exhibited the highest power density and better organic matter removal efficiency as compared to the values obtained for the other four MFCs used in this investigation and in previous investigations (Table 2).

## Cost analysis

The cost comparison of the polymer-derived ceramer and ceramic membranes with the commercial Nafion membrane was done based on retail market price of the raw materials in Germany. In order to compare the performance of MFCs in terms of power and cost, the specific power recovery per unit cost was estimated based on Eq. (8). PDC ceramer and ceramic membranes exhibited net power recovery ranging from 0.28 to 1.09 mW €$^{-1}$ with PDC:PMA10:M20-400 ceramer-based MFC being the best with net power recovery of 1.09 mW €$^{-1}$ than commercial Nafion membrane (0.54 mW €$^{-1}$). Hence, the net power recovery seems to be in favor of the PDC membranes developed in this work towards scaling up of MFC.

## Conclusion

The study investigated the polysiloxane-derived ceramer and ceramic composite membranes as separator material for MFC. The addition of 20 wt% montmorillonite and 10 wt% $H_3PMo_{12}O_{40}/SiO_2$ to polysiloxane-derived

ceramer (PDC:PMA10:M20-400) increased its hydrophilic nature and formation of hierarchical pore structure so as to cause considerable improvement of physical properties including high IEC and cation transport number and relatively low oxygen permeability coefficient. The MFC with hierarchical pore structured PDC:PMA10:M20-400 ceramer membrane generated the maximum volumetric power density of 5.66 W $m^{-3}$ and CE of $25.1 \pm 0.8\%$, which was 4- and 2-fold higher than that obtained for the MFC with PDC-400 ceramer membrane, respectively. In addition to that, power recovery per unit cost for MFC with PDC:PMA10:M20-400 ceramer membrane was double as compared with MFC having Nafion membrane. Current density of the MFC with macropore structured PDC-1000 ceramic membrane (1013 mA $m^{-2}$) was 1.6 times greater than that of the macropore structured PDC:M20-1000 ceramic membrane (633 mA $m^{-2}$), owing to the poor hydrophilic properties of the latter. This shows that the hydrophilic and porous nature could be a decidable factor for choosing proper separator material for MFC and PDC:PMA10:M20-400 ceramer being a better alternative to the commercially available Nafion membrane for its field scale applications.

**Acknowledgments** This research work was completed due to the financial support provided by the German Federal Ministry of Education and Research (BMBF), INNO INDIGO Partnership Program (01DQ15013) and German Research Foundation (DFG), Research Training Group GRK 1860 “Micro-, meso- and macroporous nonmetallic Materials: Fundamentals and Applications” (MIMENIMA), and Department of Biotechnology, Government of India (BT/IN/INNO-INDIGO/28/MMG/2015-16).

## Compliance with ethical standards

**Competing interests** The authors declare that they have no competing interests.

**Abbreviations** *MFC,* microbial fuel cell; *IEC,* ion exchange capacity; *SiOC,* silica oxycarbide; *PDC,* polymer-derived ceramics; *APTES,* aminopropyltriethoxysilane; *DO,* dissolved oxygen; *CE,* coulombic efficiency; *COD,* chemical oxygen demand

## References

1. Bose D, Gopinath M, Vijay P (2018) Sustainable power generation from wastewater sources using microbial fuel cell. Biofuels Bioprod Biorefin 12(4):559–576
2. Zhang Y, Liu M, Zhou M, Yang H, Liang L, Gu T (2019) Microbial fuel cell hybrid systems for wastewater treatment and bioenergy production: synergistic effects, mechanisms and challenges. Renew Sust Energ Rev 103:13–29
3. Wang Z, Cao C, Zheng Y, Chen S, Zhao F (2014) Abiotic oxygen reduction reaction catalysts used in microbial fuel cells. ChemElectroChem 1(11):1813–1821
4. Wang R, Yan M, Li H, Zhang L, Peng B, Sun J, Liu D, Liu S (2018) FeS2 nanoparticles decorated graphene as microbial-fuel-cell anode achieving high power density. Adv Mater 30(22):1800618
5. Zhou M, Chi M, Luo J, He H, Jin T (2011) An overview of electrode materials in microbial fuel cells. J Power Sources 196(10): 4427–4435
6. Bhowmick G, Noori MT, Das I, Neethu B, Ghangrekar M, Mitra A (2018) Bismuth doped TiO2 as an excellent photocathode catalyst to enhance the performance of microbial fuel cell. Int J Hydrog Energy 43(15):7501–7510
7. Mateo-Ramírez F, Addi H, Hernández-Fernández FJ, Godínez C, Pérez de los Ríos A, Lotfi EM, El Mahi M, Lozano Blanco LJ (2017) Air breathing cathode-microbial fuel cell with separator based on ionic liquid applied to slaughterhouse wastewater treatment and bio-energy production. J Chem Technol Biotechnol 92(3): 642–648
8. Ghadge AN, Ghangrekar M (2015) Development of low cost ceramic separator using mineral cation exchanger to enhance performance of microbial fuel cells. Electrochim Acta 166:320–328
9. Pasternak G, Greenman J, Ieropoulos I (2016) Comprehensive study on ceramic membranes for low-cost microbial fuel cells. ChemSusChem 9(1):88–96
10. Yousefi V, Mohebbi-Kalhori D, Samimi A (2018) Application of layer-by-layer assembled chitosan/montmorillonite nanocomposite as oxygen barrier film over the ceramic separator of the microbial fuel cell. Electrochim Acta 283:234–247
11. Gubler L, Scherer GG (2010) Trends for fuel cell membrane development. Desalination 250(3):1034–1037
12. Gelir A, Yargi O, Yuksel SA (2017) Elucidation of the pore size and temperature dependence of the oxygen diffusion into porous silicon. Thin Solid Films 636:602–607
13. Winfield J, Chambers LD, Rossiter J, Ieropoulos I (2013) Comparing the short and long term stability of biodegradable, ceramic and cation exchange membranes in microbial fuel cells. Bioresour Technol 148:480–486
14. Logan BE, Murano C, Scott K, Gray ND, Head IM (2005) Electricity generation from cysteine in a microbial fuel cell. Water Res 39(5):942–952
15. Ji E, Moon H, Piao J, Ha PT, An J, Kim D, Woo J-J, Lee Y, Moon S-H, Rittmann BE (2011) Interface resistances of anion exchange membranes in microbial fuel cells with low ionic strength. Biosens Bioelectron 26(7):3266–3271
16. Rahimnejad M, Bakeri G, Ghasemi M, Zirepour A (2014) A review on the role of proton exchange membrane on the performance of microbial fuel cell. Polym Adv Technol 25(12):1426–1432
17. Zhang X, Cheng S, Huang X, Logan BE (2010) The use of nylon and glass fiber filter separators with different pore sizes in air-cathode single-chamber microbial fuel cells. Energy Environ Sci 3(5):659–664
18. Neethu B, Bhowmick G, Ghangrekar M (2018) Enhancement of bioelectricity generation and algal productivity in microbial carbon-capture cell using low cost coconut shell as membrane separator. Biochem Eng J 133:205–213
19. Colombo P (2008) Engineering porosity in polymer-derived ceramics. J Eur Ceram Soc 28(7):1389–1395
20. Colombo P, Mera G, Riedel R, Soraru GD (2010) Polymer-derived ceramics: 40 years of research and innovation in advanced ceramics. J Am Ceram Soc 93(7):1805–1837
21. Liu S, Li K, Hughes R (2003) Preparation of porous aluminium oxide (Al2O3) hollow fibre membranes by a combined phase-inversion and sintering method. Ceram Int 29(8):875–881
22. Zhu W, Liu Y, Guan K, Peng C, Wu J (2019) Preparation of ZrO2 fiber modified Al2O3 membrane supports with enhanced strength and permeability. J Eur Ceram Soc 39(4):1712–1716
23. Prasad RM, Mera G, Morita K, Müller M, Kleebe H-J, Gurlo A, Fasel C, Riedel R (2012) Thermal decomposition of carbon-rich polymer-derived silicon carbonitrides leading to ceramics with high specific surface area and tunable micro-and mesoporosity. J Eur Ceram Soc 32(2):477–484

24. Lale A, Schmidt M, Mallmann MD, Bezerra AVA, Acosta ED, Machado RAF, Demirci UB, Bernard S (2018) Polymer-derived ceramics with engineered mesoporosity: from design to application in catalysis. Surf Coat Technol 350:569–586
25. Prenzel T, Guedes T, Schlüter F, Wilhelm M, Rezwan K (2014) Tailoring surfaces of hybrid ceramics for gas adsorption–from alkanes to CO2. Sep Purif Technol 129:80–89
26. Erb D, Lu K (2018) Effect of additive structure and size on SiO2 formation in polymer derived Si OC ceramics. J Am Ceram Soc 101:5378–5388
27. Fan L-p, Zhang L-l (2017) Effect of heteropolyacid and heteropolyacid salt on the performance of nanometer proton membrane microbial fuel cell. Int J Electrochem Sci 12(1):699–709
28. Gómez-Romero P, Asensio JA, Borrós S (2005) Hybrid proton-conducting membranes for polymer electrolyte fuel cells: phosphomolybdic acid doped poly (2, 5-benzimidazole)—(ABPBI-H3PMo12O40). Electrochim Acta 50(24):4715–4720
29. Ahilan V, Wilhelm M, Rezwan K (2018) Porous polymer derived ceramic (PDC)-montmorillonite-H3PMo12O40/SiO2 composite membranes for microbial fuel cell (MFC) application. Ceram Int 44(16):19191–19199
30. Müller F, Ferreira CA, Azambuja DS, Alemán C, Armelin E (2014) Measuring the proton conductivity of ion-exchange membranes using electrochemical impedance spectroscopy and through-plane cell. J Phys Chem B 118(4):1102–1112
31. Pujiastuti S, Onggo H (2016) Effect of various concentration of sulfuric acid for Nafion membrane activation on the performance of fuel cell. AIP conf proc 1711(06006):1–6
32. Hidalgo D, Tommasi T, Bocchini S, Chiolerio A, Chiodoni A, Mazzarino I, Ruggeri B (2016) Surface modification of commercial carbon felt used as anode for microbial fuel cells. Energy 99:193–201
33. Jadhav G, Ghangrekar M (2009) Performance of microbial fuel cell subjected to variation in pH, temperature, external load and substrate concentration. Bioresour Technol 100(2):717–723
34. Logan BE (2008) Microbial Fuel Cells. Wiley publication, New Jersy
35. APHA, AWWA, WPCF (1998) Standard methods for the examination of water and wastewater. American Public Health Association, Washington DC
36. Ge Z, Li J, Xiao L, Tong Y, He Z (2013) Recovery of electrical energy in microbial fuel cells: brief review. Environ Sci Technol Lett 1(2):137–141
37. Hernández-Flores G, Poggi-Varaldo H, Solorza-Feria O (2016) Comparison of alternative membranes to replace high cost Nafion ones in microbial fuel cells. Int J Hydrog Energy 41(48):23354–23362
38. Xu H, Tao S, Jiang D (2016) Proton conduction in crystalline and porous covalent organic frameworks. Nat Mater 15(7):722–726
39. Daiko Y, Kasuga T, Nogami M (2004) Pore size effect on proton transfer in sol–gel porous silica glasses. Microporous Mesoporous Mater 69(3):149–155
40. Li W-W, Sheng G-P, Liu X-W, Yu H-Q (2011) Recent advances in the separators for microbial fuel cells. Bioresour Technol 102(1):244–252
41. Atwater JE, Akse JR (2007) Oxygen permeation through functionalized hydrophobic tubular ceramic membranes. J Membr Sci 301(1–2):76–84
42. Khilari S, Pandit S, Ghangrekar MM, Pradhan D, Das D (2013) Graphene oxide-impregnated PVA–STA composite polymer electrolyte membrane separator for power generation in a single-chambered microbial fuel cell. Ind Eng Chem Res 52(33):11597–11606
43. Angioni S, Millia L, Bruni G, Ravelli D, Mustarelli P, Quartarone E (2017) Novel composite polybenzimidazole-based proton exchange membranes as efficient and sustainable separators for microbial fuel cells. J Power Sources 348:57–65
44. Jana PS, Behera M, Ghangrekar M (2010) Performance comparison of up-flow microbial fuel cells fabricated using proton exchange membrane and earthen cylinder. Int J Hydrog Energy 35(11):5681–5686